ELSEVIER

Journal of Nuclear Materials 296 (2001) 129–138

journal of nuclear materials

www.elsevier.com/locate/jnucmat

Tensile properties of candidate SNS target container materials after proton and neutron irradiation in the LANSCE accelerator ☆

K. Farrell *, T.S. Byun

Oak Ridge National Laboratory, P.O. Box 2008, Oak Ridge, TN 37831, USA

Abstract

Tensile specimens of five austenitic stainless steels and two ferritic/martensitic (f/m) steels were irradiated under spallation conditions at temperatures between 60°C and 164°C to doses between 0.4 and 11 dpa. The irradiations were performed at the Los Alamos Neutron Science Center (LANSCE) accelerator in a beam of 800 MeV protons and in the mixed spectrum of protons and spallation neutrons from a tungsten target. Tensile testing was done at room temperature at a crosshead speed of 0.005 mm/s, corresponding to a strain rate of 10^{-3} s^{-1}. All materials showed considerable irradiation hardening and loss of ductility. For EC316 LN stainless steel, which is the recommended material for construction of the spallation neutron source (SNS) mercury target container and shroud, the yield strength (0.2% offset) was increased by a factor of three at 11 dpa. This steel retained a significant uniform elongation of 6%, as did the other austenitic steels. The two f/m steels entered plastic instability failures at strains less than 1% for all doses. Published by Elsevier Science B.V.

1. Introduction

In the proposed spallation neutron source (SNS) to be built at the Oak Ridge National Laboratory, a pulsed beam of protons of 1 GeV energy and 2 mA current will impinge on a target of flowing mercury and will produce neutrons by spallation reactions in the target [1,2]. Thus the target and immediate surrounding structural materials will be exposed to intense fluxes of protons and neutrons at energies up to 1 GeV and at temperatures of about 100°C. The liquid mercury is expected to be able to bear these irradiation conditions without problem. But the tolerance limits for radiation effects in the mercury container vessel and its surrounding water-cooled shroud are less certain. It is estimated that the container vessel will undergo radiation damage of order tens of displacements per atom (dpa) per year, and substantial quantities of deleterious transmutation products will be concurrently generated in the material. Some of the transmutation products, particularly the gases hydrogen and helium, are known to exacerbate radiation damage and its effects on mechanical properties. Under spallation irradiation the transmutation rates for these gases will be orders of magnitude larger than in fission reactors, which will result in much higher concentrations of hydrogen and helium in the materials [3,4]. Such a service condition will exceed the severest irradiation conditions experienced by existing neutron scattering facilities. Although some relevant experimental data have been obtained from irradiation of materials in relatively low power proton accelerators and in neutron fission reactors, the information is not enough to qualify materials for the higher power SNS service conditions and to assess their durability for the designed lifetime of the target. More information on materials properties in the SNS irradiation environment is required. A materials R&D program that emphasizes irradiation performance and compatibility issues is underway for the SNS. Its overall scope is described in [5–7].

☆ Research sponsored by the Division of Materials Sciences and Engineering, US Department of Energy under contract DE-AC05-00OR22725 with UT-Battelle, LLC.

* Corresponding author. Tel.: +1-865 574 5059; fax: +1-865 574 0641.

E-mail address: farrellk@ornl.gov (K. Farrell).

0022-3115/01/$ - see front matter. Published by Elsevier Science B.V.
PII: S0022-3115(01)00515-3

In a similar vein, the question of materials performance under spallation irradiation conditions was faced by researchers and engineers at the Los Alamos National Laboratory in their quest to determine the feasibility of using spallation neutrons to manufacture tritium gas [8–10]. Their planned machine for accelerator production of tritium (APT) would generate neutrons by bombarding a tungsten target with a beam of 1 GeV protons. In 1995, experiments were initiated at the Los Alamos Neutron Science Center (LANSCE) to irradiate candidate APT construction materials in a beam of 800 MeV protons and spallation neutrons in order to determine their suitability for construction of the APT. ORNL requested, through a collaboration research agreement, to contribute materials of interest to the SNS for inclusion in the LANSCE-APT experiment [11]. This paper describes the ORNL-SNS materials in the experiment and summarizes their test results after irradiation.

2. Materials and specimens

Seven ORNL materials were tested. Their identities and chemical compositions are listed in Table 1. The heat treatments for these materials are described in Table 2.

The first material, and the most important one from the SNS perspective because it is the primary candidate material for the mercury container vessel and possibly the proton beam window, was type 316 LN stainless steel [11,12]. The particular heat of 316 LN chosen for these experiments was the EC316 LN alloy, where the letters EC indicate European Community. This heat has been studied under neutron irradiation conditions in fusion reactor materials programs. Several other grades of austenitic stainless steels were included as alternative candidates for container vessel materials. Of these, Superstainless AL6XN is a relatively new alloy that is stronger than 316 LN. It contains more Ni, Cr,

Table 1
Compositions of SNS materials

Material	ID Mark	Composition (wt%)									
		Bal.	Ni	Cr	Mo	Mn	Si	C	N	Nb	V	Other
EC 316 LN	E	Fe	12.2	17.45	2.5	1.81	0.39	0.024	0.067			
Superstainless AL6XN	X	Fe	24.0	20.5	6.3	0.40	0.40	0.02	0.22			
HTUPS 316 (#AX5)	H	Fe	16.2	13.9	2.46	2.04	0.12	0.076	0.021	0.15	0.52	0.27 Ti
Single crystal stainless steel	S	Fe	21.2	16.3								
Single crystal stainless steel rolled and recrystallized to polycrystal state	R	Fe	21.2	16.3								
Modified 9Cr–1Mo steel (Ht. 30176)	M	Fe	0.09	8.32	0.86	0.48	0.15	0.092	0.055	0.06	0.20	
9Cr–2WVTa steel (Ht. 3791)	V	Fe	<0.01	8.90	0.01	0.44	0.21	0.11	0.021	<0.01	0.23	2.01 W; 0.06 Ta

Table 2
Heat treatments of SNS materials

Material	Heat treatment
EC 316 LN	Annealed 1 h at 950°C in vacuum
Superstainless AL6XN	Annealed 30 min at 1110°C in helium, fast cool
HTUPS 316(#AX5)	Annealed 12 min at 1200°C in helium, fast cool
Single crystal stainless steel	Annealed 30 min at 950°C in vacuum
Single crystal stainless steel rolled and recrystallized to polycrystal state	Cold rolled 50% then annealed 30 min at 950°C in vacuum
Modified 9Cr–1Mo steel (Ht. 30176)	Wrapped in Zr foil and annealed 30 min at 1050°C in helium, fast cool; reheated 1 h at 760°C, fast cool
9Cr–2WVTa steel (Ht. 3791)	Wrapped in Zr foil and annealed 30 min at 1050°C in helium, fast cool; reheated 1 h at 750°C, fast cool

Mo, and N than 316 LN, and claims outstanding resistance to aqueous corrosion. The high temperature ultra-fine precipitate steel (HTUPS) alloy is a modified 316 stainless steel recently developed at ORNL. These three austenitic steels were irradiated in annealed conditions.

To explore the effects of grain boundaries, which may become susceptible to liquid metal embrittlement in mercury or to intergranular helium embrittlement, a special austenitic stainless steel was included in both a single crystal condition free of grain boundaries and in a polycrystalline condition achieved by rolling and recrystallization of the original single crystals.

European researchers have suggested ferritic/martensitic (f/m) steels for construction of the target container of their proposed European spallation source because they are stronger than austenitic steels, have greater thermal conductivities, which facilitates removal of irradiation-induced heat, and have good resistance to liquid metal embrittlement. Their increased strength comes at a cost of reduced ductility. Moreover, like all ferritic steels, they suffer a ductile-to-brittle transition (DBTT) over a narrow temperature range, usually well below room temperature, but which is raised by irradiation. Ferritic/martensitic steels based on 9Cr–1Mo alloys, which have low DBTTs and show promise of greatly improved resistance to radiation-affected DBTT shifts, are undergoing trials for applications in reactor core regions at moderately elevated temperatures. To compare the radiation responses of f/m steels directly with austenitic stainless steels under a common spallation-type irradiation field and at low temperature of interest to the SNS, we included a regular modified 9Cr–1Mo steel and a low-activation 9Cr–2W–V–Ta steel in the APT experiment. These two steels were irradiated in their quenched-and-tempered states.

These materials were irradiated in the forms of various kinds of test specimens: miniature tensile specimens, miniature fatigue specimens, TEM specimens, stressed ring specimens and creep specimens. This report describes only data obtained from S-1 type miniature tensile specimens. The S-1 is not an engineering standard specimen, and data obtained from it should not be considered as being suitable for quantitative engineering design purposes. It is shown in Fig. 1. Its gauge section dimensions are 5 mm long, 1.2 mm wide, and 0.25 mm thick. This small specimen design was chosen by the APT experiment group to maximize the number of specimens that could be irradiated in the narrow, Gaussian-shaped beam, and to minimize the flux gradients along the specimen gauge lengths. Data from 41 S-1 specimens of austenitic steels and 23 f/m steel specimens from ORNL are presented in this report.

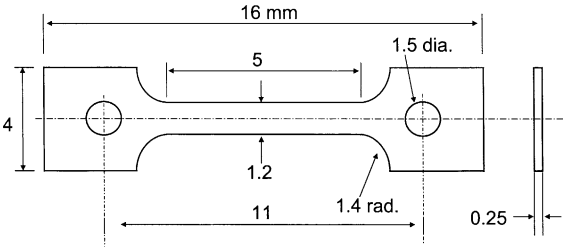

Fig. 1. Dimensions of APT S-1 specimen.

3. Irradiation conditions

3.1. Fluence and dpa

A full description of the irradiation conditions is given in [13,14]. The ORNL specimens were sealed, along with specimens from other laboratories, in stainless steel envelopes and were stacked in arrays of horizontal tubes about 160 mm long through which cooling water flowed between the envelopes. The specimens reported herein were irradiated in tubes at two different locations in the experiment labeled Inserts 17A and 18C. (See Fig. 1 in [13] or Fig. 2 in [14] for a sketch of the Insert locations.) Insert 17A lay directly in the path of the incoming proton beam in front of the tungsten target rods which were in Insert 18A. Insert 18C was downstream from 18A.

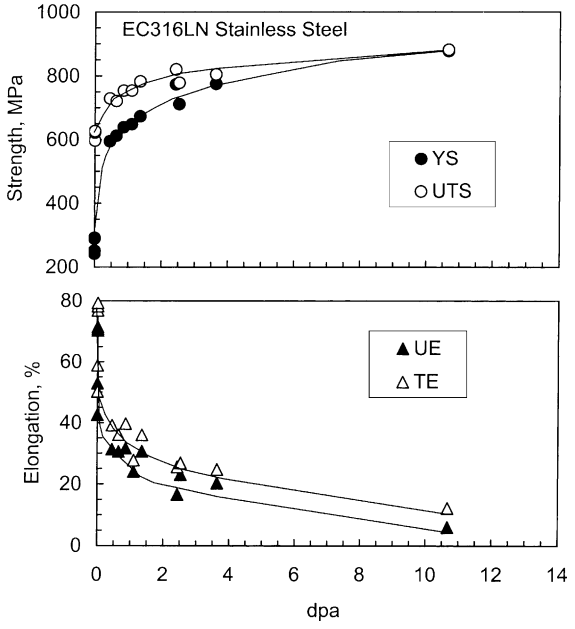

Fig. 2. Dose dependence of tensile properties of annealed EC316 LN stainless steel.

Table 3
Tensile properties of all materials

Materials	Irrad. posn. I–T–E[a]	ID Mark	dpa	YS (MPa)	UTS (MPa)	UE (%)	TE (%)
EC316 LN		E15	0	292	598	52.9	58.8
		E16	0	288	597	42.6	50.2
	18C-29-3	E7	0.4	595	729	31.3	39.2
	18C-29-3	E8	0.6	612	721	30.5	36.0
	17A-1-3	E1	0.9	639	754	31.6	39.7
	18C-27-4	E4	1.1	648	754	24.0	27.7
	18C-29-3	E9	1.4	673	783	30.6	36.0
	17A-1-3	E2	2.4	773	820	16.6	25.5
	18C-27-4	E5	2.5	711	778	23.0	26.8
	18C-27-4	E6	3.6	775	805	20.3	24.7
	17A-1-3	E3	10.7	877	881	6.0[b]	12.2
AL6XN		X20	0	272	642	46.7	52.1
		X21	0	285	661	48.4	52.3
	18C-29-3	X10	0.4	610	753	32.5	38.5
	18C-29-3	X11	0.6	635	759	32.6	36.9
	17A-1-3	X2	0.9	650	765	32.4	37.6
	18C-27-4	X7	1.1	647	763	28.9	32.9
	18C-29-3	X12	1.4	686	781	29.0	34.1
	17A-1-3	X3	2.4	786	840	18.3	24.4
	18C-27-4	X8	2.5	715	787	30.4	33.5
	18C-27-4	X9	3.6	783	823	22.7	28.5
	17A-1-3	X5	10.7	980	989	0.5	13.3
HTUPS316		H11	0	175	535	45.6	49.4
		H12	0	185	506	34.5	38.8
		H13	0	176	511	38.6	42.9
		H14	0	184	516	35.5	40.3
		H15	0	177	512	32.9	35.9
	18C-29-3	H4	0.4	571	662	25.3	29.1
	18C-29-3	H5	0.6	610	685	22.2	25.5
	18C-29-3	H6	1.1	724	737	19.8	22.5
	18C-27-4	H1	1.2	658	704	21.9	25.1
	18C-27-4	H2	2.8	724	741	10.6	13.4
	18C-27-4	H3	4.0	791	767	12.1[b]	15.4
Single crystal stainless		S2	0	163	419	28.1	34.8
	17A-1-3	S3	0.9	574	580	28.9	33.9
	17A-1-3	S4	2.5	628	628	15.0[b]	17.2
	17A-1-3	S5	11.3	591	621	22.2	30.6
Recryst. single crystal		R6	0	113	453	50.6	55.2
	17A-1-3	R3	0.9	604	647	24.3	29.7
	17A-1-3	R4	2.5	736	694	12.7[b]	16.3
	17A-1-3	R5	11.3	641	659	10.9	15.7
9Cr–2WVTa		V12	0	604	716	4.7	11.7
		V13	0	588	727	7.5	14.8
		V15	0	496	638	7.2	13.7
	18C-27-4	V4	0.5	887	900	0.6	7.1
	18C-29-3	V7	0.7	917	926	0.5	6.4
	17A-1-3	V1	0.8	900	909	0.7	5.3
	18C-27-4	V5	0.9	920	938	0.5	5.7
	18C-29-3	V8	1.3	927	927	0.4	5.8
	18C-29-3	V9	1.8	979	979	0.4	5.7
	17A-1-3	V2	2.2	980	992	0.4	5.4
	18C-27-4	V6	2.5	967	977	0.5	5.8
	17A-1-3	V3	10.1	1170	1214	0.8	4.8

Table 3 (Continued)

Materials	Irrad. posn. I–T–E[a]	ID Mark	dpa	YS (MPa)	UTS (MPa)	UE (%)	TE (%)
Modified 9Cr–1Mo		M12	0	558	692	7.6	16.9
		M13	0	554	668	7.9	16.1
		M20	0	560	697	8.0	16.2
	18C-27-4	M4	0.5	841	884	0.4	7.2
	17A-1-3	M1	0.8	873	887	0.5	5.0
	18C-27-4	M5	0.9	871	910	0.5	6.2
	18C-29-3	M8	1.3	905	932	0.5	6.2
	18C-29-3	M9	1.8	931	954	0.6	5.9
	17A-1-3	M2	2.2	954	958	0.4	4.6
	18C-27-4	M6	2.5	942	973	0.5	6.1
	17A-1-3	M3	10.1	1183	1196	0.5	0.7

[a] Insert number, tube number, envelope number.
[b] Strain to necking.

The quasi-continuous proton beam had an energy of 800 MeV and an average current of 1 mA. It was of circular cross-section with a diameter of about 80 mm and a peak flux at its center of 3.7×10^{18} p m^{-2} s^{-1}. The flux profile in the incident beam was Gaussian with a 2σ of about 35 mm. Irradiation was begun 1 September, 1996 and ran to 24 July 1997, with a break from 3 November 1996 to 26 March 1997. The accumulated on-line time was 3614 h. Because of the Gaussian beam profile and its dispersal as it became scattered downstream, there was spatial variation of spectra, dose, and temperature at each Insert and within each tube. Specific irradiation exposure values for each specimen depended on its distance along the length of the beam axis and its horizontal and vertical distances from the axis. These data are given in detail in Table 4 of [14], and consist of values of dpa, He production, and H production, proton fluence, and neutron fluences in four energy groups. They are derived from the measurements and calculations of James et al. [13] for the APT experiment. Despite the fact that the Insert 17A specimens were irradiated upstream in front of the tungsten target rods and the Insert 18C specimens were irradiated downstream behind the target bundle, there was sufficient spherical scattering of neutrons that the neutron and proton spectra at both Inserts were not greatly dissimilar. The tensile properties were found to correlate well with dpa. Therefore, and for the sake of brevity, only the dpa values are used herein. These have an approximate uncertainty of 25%. Helium and hydrogen concentrations were measured for the steels and nickel alloys irradiated in the APT experiment [15]. The ratio of He/dpa was found to be about 150 appm/dpa, and the ratio of H/dpa was roughly 1500.

3.2. Irradiation temperature

The LANSCE-APT project team has released some preliminary temperature data for the ORNL-SNS specimens. In our upstream position, Tube 1 in Insert 17A, the average maximum temperature was 117–164°C. This tube received larger doses than Insert 18C in which our specimens in Tube 27 saw an average maximum temperature of 58–67°C, and those in Tube 29 experienced an average maximum temperature of 73–83°C.

4. Tensile test conditions

To protect the tiny specimens from accidental damage during remote handling into the tensile machine, and to avoid deformation occurring outside the gage section at the pinholes during the test, a specially designed sliding carriage was used to support the specimen during insertion and testing. The load was not applied through the pinholes. It was applied under the specimen shoulders through ledges machined into the sliding carriage that were shaped to match the radius of the specimen shoulders. Gauge thicknesses and widths were measured on the specimens before they were irradiated. A generic, unirradiated gauge length of 5 mm was taken as the reference gauge length. The load cell and displacement values and rates were calibrated to NIST standards.

Tensile testing was performed at room temperature in a hard, screw-driven machine, ATC Model #FIM-B4 operating under computer control at a crosshead speed of 0.005 mm/s, corresponding to a nominal strain rate of 10^{-3} s^{-1}. Unirradiated control specimens were tested in the same machine in the same campaign as the irradiated specimens. Plastic elongation values were determined from crosshead displacement measurements after allowances were made for elastic displacements and compliance in the specimen holding train. Yield strengths were read at 0.2% plastic strain unless there was a yield point drop, in which case the yield strength was read at the base of the drop.

5. Results and discussion

All the tensile test data are listed in Table 3, and selected data are depicted in Figs. 2–7. Because the data were obtained from two different Inserts with different irradiation temperatures and moderately different irradiation particle spectra, we first examined the data thoroughly to seek any differences in properties that might be attributed to these differences in exposure factors. We found no signs of differences due to either factor. Therefore, in the Figures, no attempt is made to label the data points from the two Inserts. If desired, the reader can distinguish them by checking the Insert numbers in the irradiation position column in Table 3.

Except for a single specimen of 9Cr–1Mo steel, none of the materials after irradiation were brittle in the sense that ceramic materials are frangible. On the contrary, the specimens failed with highly ductile, chisel-edge-type fractures. They all lost toughness, as witnessed by decreasing areas under their tensile curves. There were no signs of intergranular separation by helium embrittlement.

The tensile properties of the EC316 LN austenitic steel are presented as functions of irradiation dose in dpa in Fig. 2. With increasing dose the strengths increased and the elongations decreased in smoothly varying manner. More than half the values of the changes occurred below a dose of 1 dpa. At a dose of 10.7 dpa, the yield strength was raised by a factor of almost 3. The UTS was increased by a factor of about 1.5, reflecting reduced work hardening as a result of irradiation. Reduced work hardening translates to reduced uniform elongation. At the highest dose of 10.7 dpa, a small degree of work hardening capacity was retained, and the uniform elongation was 6%.

For the most part, the irradiation responses of the other austenitic alloys were very similar to those of EC316 LN steel despite their large differences in chemical compositions. Their tensile properties are plotted in Fig. 3 overlaid on trend data bands for annealed 316 stainless steel irradiated at temperatures below 200°C in fission reactors [12,16]. The properties are fully compatible with the trend bands, except that the yield strengths and UTS values for the EC316 LN and AL6XN steels at 10–11 dpa are somewhat higher than the bands. A reasonable assumption is that this extra strengthening is due to the high gas contents generated in these irradiations, as demonstrated in austenitic alloys irradiated with helium and hydrogen ions [17]. It is well known that the presence of helium can stimulate the formation of radiation displacement damage microstructure. Also, the development of small quantities of entrapped helium from decay of dissolved tritium can cause measurable hardening. However, the contribution of hardening from the gases is usually small compared to the hardening from displacement damage, and it takes large quantities of helium, 5000 appm or more, and even larger quantities of hydrogen coexisting with the helium,

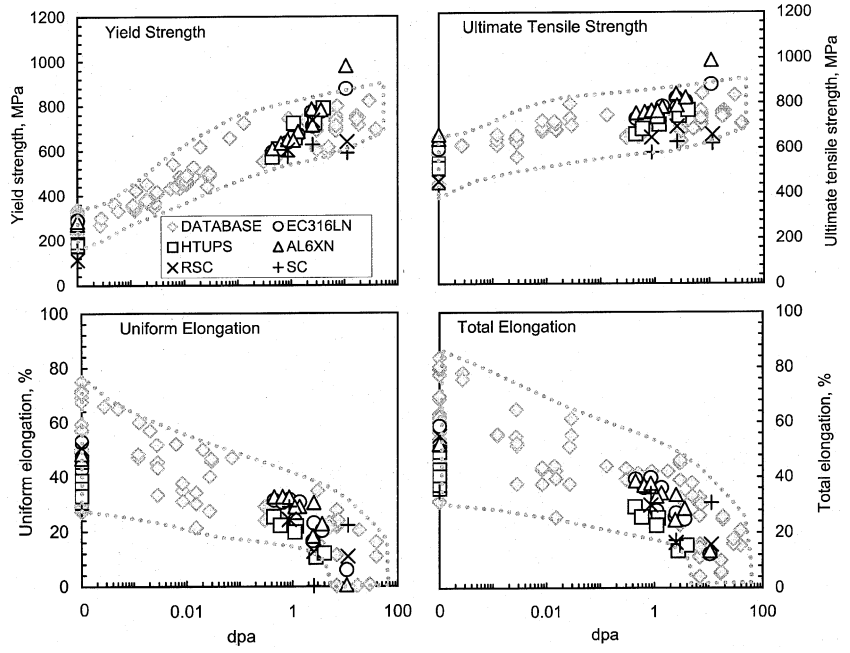

Fig. 3. Tensile properties of the austenitic alloys overlaid on data bands for fission reactor irradiated 316 stainless steel irradiated and tested at temperatures between 25°C and 200°C.

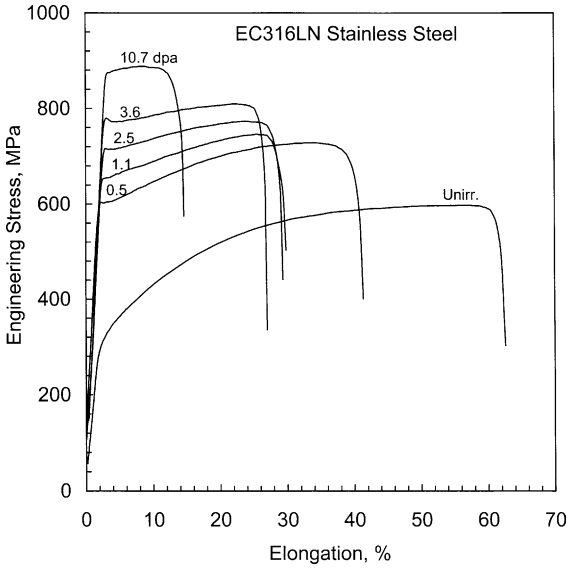

Fig. 4. Examples of tensile test curves for EC316 LN steel.

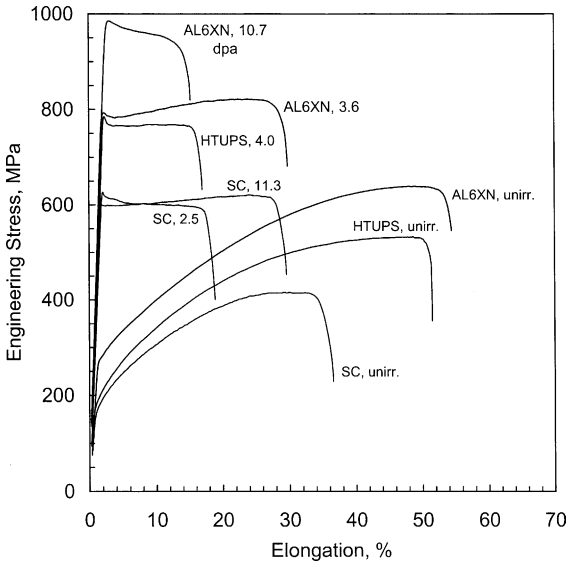

Fig. 5. Selected tensile test curves for austenitic alloys.

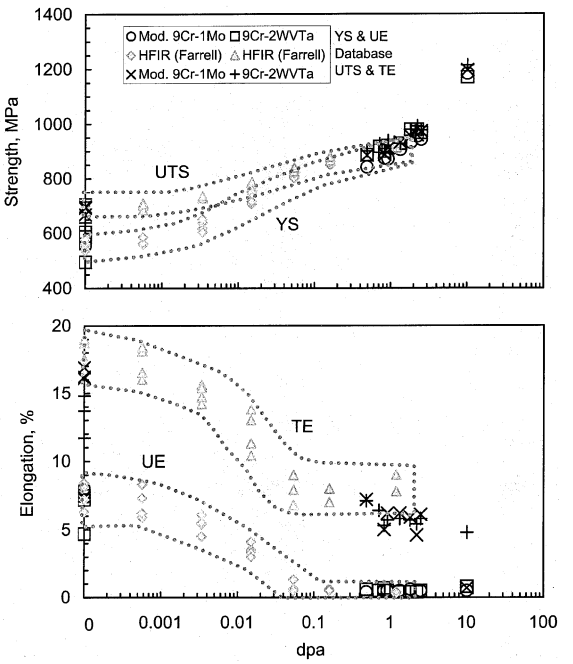

Fig. 6. Dose dependence of f/m alloys overlaid on data bands for the same alloys irradiated in the HFIR at about 60°C.

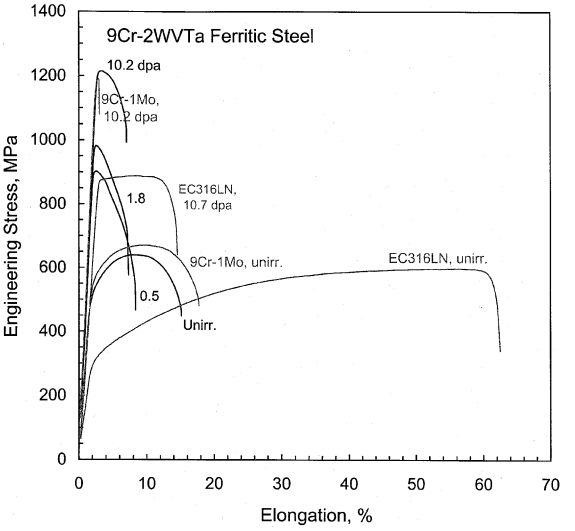

Fig. 7. Comparison of tensile curves for the f/m steels with those for EC316 LN stainless steel.

to discern gas hardening from displacement hardening when both sources of hardening are generated simultaneously during ion bombardment [17]. The gas contents in the EC316 LN and AL6XN steels at 10.7 dpa are of order 1600 appm helium and 16,000 appm hydrogen, and are thus marginal for detectable strengthening contribution. Moreover, the single crystal (SC) alloy and its rolled and recrystallized companion material (RSC) should also have the same gas contents as the EC316 LN and AL6XN steels after doses of 11.3 dpa, yet they do not display a strengthening surge. Thus, if the gases are the cause of the surges, they must be more effective than in the ion-bombarded steels, and they must be acting in concert with foreign elements present in the steels but not in the single crystal alloy.

In spite of the apparent commonality of irradiation responses for the various austenitic alloys in Fig. 3, there are subtle differences that become more visible when the

tensile test curves are compared. The tensile test curve not only contains the loads and extensions that provide the engineering tensile properties data, it holds a record of the deformation processes that affect the shape of the curve. Thus, the curve shape can be interpreted to give subtle information on the deformation processes controlling the tensile properties. Fig. 4 shows representative engineering stress–strain curves for the EC316 LN austenitic stainless steel. To avoid overcrowding the figure, many curves are omitted. The missing curves can be viewed in [14], and they fit smoothly between the displayed curves, indicating no obvious discontinuities in the progressive change in shape with dose. Considerable radiation-induced strengthening and loss in elongation are clearly seen in the curve at the lowest dose of 0.5 dpa, and continue at reduced rate with increasing dose. The curves also show the introduction of yield point drops followed immediately by short, dished regions reminiscent of brief Luders strain regions. Subsequent work hardening, indicated by the slope of the curve in the early regions of the uniform elongation portion, is significantly less than for the unirradiated specimen at equal elongation value. Reduction in work hardening translates to reduction in uniform elongation.

The pattern of tensile curve shape changes displayed by the EC316 LN alloy is duplicated by the other four austenitic stainless steels, with a few additional features, as illustrated in Fig. 5. One feature is shown by the AL6XN alloy. When irradiated to doses up to about 4 dpa its tensile curves are similar to those for EC316 LN alloy. But at 10.7 dpa it displayed negative work hardening, in engineering terms. (In true stress-true strain parameters the work hardening rate is still positive but is greatly reduced). That is, immediately after yield it underwent about 10% elongation under decreasing stress before entering true necking failure. This type of pseudo uniform strain at constant or slowly decreasing load has been dubbed 'strain to necking' (STN) by Horsten and De Vries [18]. Observing the specimen with binoculars through the cell window we saw that the STN occurred with uniform reduction in specimen width. A similar event happened in HTUPS steel at its highest dose of 4 dpa, where about 12% strain to necking was registered at constant engineering stress. In the single crystal steel at 2.5 dpa there was about 15% STN under decreasing load, yet at 11.3 dpa the alloy showed a small positive work hardening and 22% uniform elongation.

These irradiation-induced features of the stress–elongation curve are not peculiar to the spallation-irradiated materials; they are seen in fission-irradiated materials, too [16,18,21]. We believe they are symptomatic of heterogeneous plastic deformation on a microscopic scale, otherwise known as dislocation channeling [19,20]. Generally, those metals that normally deform by dislocation tangling and cell formation in their unirradiated conditions tend to deform by dislocation channeling after irradiation. Austenitic stainless steel has low stacking fault energy and normally it deforms by strongly planar slip; after irradiation, the deformation remains largely on the primary slip planes but changes to microtwinning [22,23]. Confinement of the strain in the channels or twin bands gives high strains in the channels and twin bands but seriously reduces bulk work hardening and bulk elongation. In a seeming paradox, deformation occurring during necking or during STN is increased, presumably because the change from uniaxial stress to multiaxial stress as the gauge section is constricted either disrupts the bands or brings into play many more channels and bands that had been dormant under the uniaxial state.

The impact of reduced ductility in service on the development of guidelines and standards for the design of reactor components is being addressed for fusion reactor internals [24]. However, it is based on the assumption that the plastic strains involved are uniform strains. It does not consider STN. At high doses, the type of strain transition where uniform elongation is exhausted at some threshold dose and is replaced by substantial STN is becoming more the rule than the exception. It is well established in reactor-irradiated austenitic steels [16,18,21]. For spallation irradiations, it is reported by Maloy et al. [10,25] for 304L and 316L grades irradiated in the same spallation irradiation experiment as the present work. It poses a dilemma for engineering assessment. Technically we cannot call this strain uniform elongation because the yield strength and UTS values are coincident, but effectively it is uniform elongation. Whether it has engineering usefulness is not clear. It is also not clear where the threshold dose lies, or what controls it. In the present work STN seems to be independent of unirradiated yield strength but may be dependent on chemical composition. The EC316 LN steel did not cross the threshold at 10.7 dpa but the AL6XN steel did. The HTUPS steel was on the verge of crossing at 4 dpa, and the purer single crystal alloy vacillated between 3 and 11 dpa. In Maloy's alloys the threshold was about 3 dpa, and it decreased with increasing test temperature between 50°C and 160°C [25].

The tensile properties of unirradiated and irradiated f/m steels are presented in Fig. 6. They are superimposed on unpublished data obtained by the current authors for the same steels irradiated in the high flux isotope reactor (HFIR) at about 60°C. The unirradiated f/m steels were stronger than the austenitic steels and less ductile. After irradiation they showed significant radiation-induced hardening. At the highest dose of 10 dpa, their yield strengths were raised by a factor of 2. The irradiated f/m specimens had little or no uniform plastic strain even for the lowest dose of 0.5 dpa. Rather, at yield they entered immediately into plastic instability failure (necking) but with significant necking strain that registered as total

elongation. Both of these steels displayed almost identical radiation responses per unit dose. For doses above about 2 dpa they displayed more strengthening than extrapolations of the HFIR data would indicate, and at 10 dpa they were markedly stronger. This departure could be a result of the much larger gas contents.

Some tensile test curves for the 9Cr–2WVTa steel are presented in Fig. 7 together with several curves for the 9Cr–1Mo and austenitic EC316 LN steel for comparison. The prompt plastic failure at yield is obvious. The 9Cr–1Mo curves were almost identical to the 9Cr–2WVTa curves at equal doses, except for the 10.2 dpa specimen, which is shown and which failed in a truly brittle manner in contrast to the counterpart 9Cr–2WVTa specimen that produced more necking strain. This is the only sign that the 9Cr–2WVTa steel might be a little tougher than 9Cr–1Mo after irradiation. The f/m tensile curves offer no guidance to the deformation mechanisms, although the sudden plastic instability type failures are characteristic of strain localization.

As a group, the f/m steels compare unfavorably with the austenitic steels with regard to retained ductility. Also, given that the properties of ferritic alloys are very much more sensitive to strain rate and size effects than the properties of austenitic alloys, and that the measured large irradiation-induced increases in strengths of the f/m steels can be taken as indices of upshifts in their DBTTs, the disparity with austenitic alloys widens considerably. It is considered that the f/m steels would be an unsuitable choice for construction of the SNS target vessel, which must sustain pulsed shock loads. Type 316 LN stainless steel is the most prudent choice.

6. Conclusions

The tensile properties of candidate SNS target container steels after proton and spallation neutron irradiation at temperatures between 60°C and 164°C in the LANSCE accelerator are described. All test materials showed significant radiation hardening and loss in ductility in agreement with databases for materials irradiated in fission reactors, except for more radiation strengthening at high dose, presumed to be due to higher gas contents. Loss of ductility in the austenitic alloys is attributed to strain localization during deformation. Austenitic stainless steels were the most resistant to loss of ductility after irradiation, especially the EC316 LN alloy, which retained a uniform elongation of 6% at room temperature after irradiation to a maximum dose of 11 dpa. Ferritic/martensitic steels showed prompt necking at less than 1% plastic strain even at 0.5 dpa, and they are judged unsuitable for the SNS application.

Acknowledgements

We much appreciate this participation in the LANL-APT materials irradiation experiment. Cooperation was initiated by Dr L.K. Mansur of ORNL with Dr W. Sommer of LANL, who arranged for ORNL's participation. Dr S.A. Maloy of LANL coordinated the incorporation of the ORNL-SNS specimens and worked closely with us on the project. We thank Dr M.R. James of LANL for his cooperation in deriving the fluence and dpa data.

References

[1] T.A. Gabriel, J.M. Barnes, L.A. Charlton, J. Distefano, K. Farrell, J. Haines, J.O. Johnson, L.K. Mansur, S.J. Pawel, M. Siman-Tov, R. Taleyarkhan, T.J. McManamy, M. Rennich, in: Proceedings of the Topical Meeting on Nuclear Applications of Accelerator Technology, Albuquerque, NM, November 16–20, 1997, Am. Nucl. Soc., p. 288.

[2] J.R. Haines, T.A. Gabriel, T.J. McManamy, in: Proceedings of the Second International Topical Meeting on Nuclear Applications of Accelerator Technology, Gatlinburg, TN, September 20–23, 1998, Am. Nucl. Soc., p. 222.

[3] M.S. Wechsler, M.H. Barnett, D.J. Dudziak, L.K. Mansur, L.A. Charlton, J.M. Barnes, J.O. Johnson, in: Proceedings of the Symposium on Materials for Spallation Neutron Sources, Orlando, FL, February 10–12, 1997, TMS, Warrendale, PA, 1998, p. 23.

[4] E.J. Pitcher, P.D. Ferguson, G.J. Russell, R.E. Prael, D.G. Madland, J.D. Court, L.L. Daemen, M.S. Wechsler, in: Proceedings of the Symposium on Materials for Spallation Neutron Sources, Orlando, FL, February 10–12, 1997, TMS, Warrendale, PA, 1998, p. 15.

[5] L.K. Mansur, J.R. Distefano, K. Farrell, E.H. Lee, S.J. Pawel, M.S. Wechsler, in: Proceedings of the Topical Meeting on Nuclear Applications of Accelerator Technology, Albuquerque, NM, November 16–20, 1997, Am. Nucl. Soc., p. 301.

[6] L.K. Mansur, in: Proceedings of the American Nuclear Society Meeting, Boston, MA, June 6–10, 1999, TANSAO, vol. 80, 1999, p. 94.

[7] S.J. Pawel, J.R. Distefano, L.K. Mansur, K. Farrell, J.P. Strizak, T.S. Byun, in: Proceedings of the Third International Topical Meeting on Nuclear Applications of Accelerator Technology, Long Beach, CA, November 14–18, 1999, Am. Nucl. Soc., p. 117.

[8] W.F. Sommer, in: Proceedings of the International Workshop on Spallation Materials Technology, Oak Ridge, TN, USDOE CONF-960451, April 23, 1996, p. 3.2-1.

[9] S.A. Maloy, W.F. Sommer, R.D. Brown, J.E. Roberts, J. Eddleman, E. Zimmermann, G. Willcutt, in: Proceedings of the Symposium on Materials for Spallation Neutron Sources, Orlando, FL, February 10–12, 1997, TMS, Warrendale, PA, 1998, p. 131.

[10] S.A. Maloy, Los Alamos National Laboratory Report TPO-RGN-0013, January 1999.

[11] K. Farrell, Oak Ridge National Laboratory Report SNS/TSR-0036, March 1998.
[12] K. Farrell, L.K. Mansur, in: Proceedings of the International Workshop on Spallation Materials Technology, Oak Ridge, TN, USDOE CONF-960451, April 23, 1996, p. 3.3-1.
[13] M.R. James, S.A. Maloy, W.F. Sommer, P. Ferguson, M.M. Fowler, K. Corzine, in: Proceedings of the 2nd International Topical Meeting on Nuclear Applications of Accelerator Technology, Gatlinburg, TN, September 20–23, 1998, Am. Nucl. Soc., p. 605 (and E-mail correspondence with M.R. James, S.A Maloy.
[14] K. Farrell, T.S. Byun, Oak Ridge National Laboratory Report SNS/TSR-193, May 2000.
[15] B.M. Oliver, F.A. Garner, S.A. Maloy, W.F. Sommer, P.D. Ferguson, M.R. James, in: Effects of Radiation on Materials, 20th International Symposium, ASTM STP 1405, Am. Soc. Test. Mater., West Conshohocken, PA, in press.
[16] J.E. Pawel, A.F. Rowcliffe, G.E. Lucas, S.J. Zinkle, J. Nucl. Mater. 239 (1996) 126.
[17] J.D. Hunn, E.H. Lee, T.S. Byun, L.K. Mansur, J. Nucl. Mater. 282 (2000) 131.
[18] M.G. Horsten, M.I. DeVries, in: Effects of Radiation on Materials, 17th International Symposium, ASTM STP 1270, Am. Soc. Test. Mater., West Conshohocken, PA, 1996, p. 919.
[19] F.A. Smidt, Naval Research Laboratory Report 7078, June 3, 1970.
[20] M.S. Wechsler, in: The Inhomogeneity of Plastic Deformation, Am. Soc. Metals, 1971 (Chapter 2).
[21] A.F. Rowcliffe, S.J. Zinkle, J.F. Stubbins, D.J. Edwards, D.J. Alexander, J. Nucl. Mater. 258–263 (1998) 183.
[22] S.M. Bruemmer, J.I. Cole, R.D. Carter, G.S. Was, Mater. Res. Soc. Symp. Proc. 439 (1997) 437.
[23] E.H. Lee, T.S. Byun, J.D. Hunn, K. Farrell, L.K. Mansur, these Proceedings, p. 183.
[24] S. Majumdar, Fus. Eng. Des. 29 (1994) 158.
[25] S. Maloy, M.R. James, G. Willcutt, W.F. Sommer, M. Sokolov, L.L. Snead, M.L. Hamilton, F. Garner, these Proceedings, p. 119.